Tunable Second-Order Sideband Effects Based on Dual-Species BEC-Optomechanical Systems

Li-Wei Liu[a,b,*], Guo-Heng Zhang[a], Xiang-Li Wang[a], Xiu-Jia An[a] and Hai-Yan Jiao[a]

[a] *College of Electrical Engineering, Northwest Minzu University, Lanzhou 730000, China*
[b] *Key Laboratory for Electronic Materials of the State Ethnic Affairs Commission of PRC, Northwest Minzu University, Lanzhou 730000, China*

Received: 10.07.2022 & Accepted: 24.11.2022

Doi: 10.12693/APhysPolA.143.89 *e-mail: liuliw@xbmu.edu.cn

We theoretically investigate a second-order optomechanically induced transparency process of a cigar-shaped dual-species Bose–Einstein condensate with nonlinear collisions trapped inside an optomechanical cavity. We find that atomic collisions provide linear couplings, which facilitate the mechanical mixing of the dual-species Bose–Einstein condensate. We derive analytical expressions of the output transmission intensity of the probe field and the dimensionless amplitude of the second-order sideband. The numerical results show that the transmission intensity and the dimensionless amplitude of the second-order sideband can be controlled by the control field intensities, the effective detuning, and the effective coupling strength of the Bogoliubov mode of the dual-species Bose–Einstein condensate and optical mode. Furthermore, the interspecies and intraspecies interactions are also used to control the transmission intensity and the dimensionless amplitude of the second-order sideband.

topics: cavity optomechanical system, dual-species Bose–Einstein condensate, second-order sideband

1. Introduction

Cavity optomechanical systems (COMS) have attracted considerable attention and are developing rapidly, and the mechanical effects of light on both mesoscopic and macroscopic mechanical oscillations have been described [1–4]. In the field of COMS, there has been a great surge of interest in various systems, such as an optical field with a movable end mirror [5–8], nanomechanical cantilevers [9, 10], a micro-mechanical membrane oscillating [11, 12], vibrating microtoroids [13, 14], atomic ensembles [15–18], and a Bose–Einstein condensate (BEC) inside two fixed cavities [19–21]. Recently, much attention is also focused on the studies of the hybrid COMS with atomic ensembles or BEC, in which the excitation of a collective mode of the cold atomic ensembles or BEC (the so-called Bogoliubov mode) plays the role of the vibrational mode of the moving mirror [22–24].

Moreover, a lot of interesting phenomena have been proved theoretically and experimentally in the hybrid COMS, such as optomechanically induced transparency (OMIT) [25–27], normal mode splitting [28, 29], optomechanical storage [30, 31], quantum-coherent coupling [31–34], quantum entanglement generation [35–38], the second-order sideband (SS) or even higher-order sidebands (HS) effect [39–44], and so on. Furthermore, one of the most important features of this hybrid COMS is inherent nonlinearity, which is caused by the mutual interaction between the cavity field and the matter inside (the atomic ensemble or the Bogoliubov mode) [45, 46]. In addition, there is also another nonlinearity induced by an atom–atom interaction in hybrid COMS containing the cold atomic ensemble or BEC [47, 48]. In recent years, the hybrid COMS could be used to study a variety of exotic effects due to the nonlinear nature of interactions, especially OMIT and the SS effect. However, even though the nonlinear SS effect is much weaker in comparison with the probe field, the generation of nonlinear OMIT effects and the SS signals is useful for more flexible control of light in the hybrid COMS.

Motivated by these exciting features, we consider a cigar-shaped dual-species Bose–Einstein condensate (DBEC) trapped in an optical cavity [49–56]. In addition to considering the interspecies and intraspecies interaction, we give the full model of a DBEC cavity optomechanical system, which is driven by an external laser. There are many advantages of using DBEC trapped inside an optomechanical cavity. Firstly, it changes the effective oscillation frequencies of both the cavity mode and the Bogoliubov mode of DBEC and also affects their relaxation times [52–54]. Furthermore, the coupling interaction and interspecies and in-

traspecies interaction strengths can use Feshbach resonances to realize [55, 56]. More importantly, it can make the system controllable to obtain OMIT and the SS effects.

In this paper, we consider a cigar-shaped DBEC coupled with an optical cavity, and, taking into account the discrete mode approximation, we give an effective COMS model with the collective DBEC modes playing the role of mechanical oscillators in Sect. 2. We give the analytic expression of the transmission intensity $|t_p|^2$ of the probe field and the dimensionless amplitude η_s of SS by the quantum-Langevin equations. Based on the analytical expressions, the numerical results in Sect. 3 show that the effect of the transmission intensity and the dimensionless amplitude of SS can be controlled effectively by the control cavity field intensities, the effective detuning, the effective coupling strength of the optical field with the Bogoliubov mode of the collective oscillation of the dual-species BEC, and interspecies and intraspecies interaction strengths. Finally, we give a summary in Sect. 4.

2. The model of the system

The cavity optomechanical system we considered is shown schematically in Fig. 1, and consists of a cigar-shaped DBEC inside a single-mode, high-finesse Fabry-Pérot cavity with length L, both mirrors or which are fixed. The effective Hamiltonian of DBEC and cavity in the frame rotating at a driving field frequency ω_{pu} is [55–57]

$$\begin{aligned}\hat{H} = &\sum_{i,j\neq i}^{2}\hbar\left[\frac{\omega_i}{2}\left(\hat{P}_i^2+\hat{Q}_i^2\right)+U_{ii}\hat{Q}_i^2+\frac{U_{ij}}{2}\hat{Q}_i\hat{Q}_j\right]\\&+\hbar\sum_{i=1}^{2}\xi_i\,\hat{c}^{\dagger}\hat{c}\,\hat{Q}_i+\hbar\Delta_c^{'}\,\hat{c}^{\dagger}\hat{c}+\mathrm{i}\hbar\,\varepsilon_{pu}\left(\hat{c}^{\dagger}-\hat{c}\right)\\&+\mathrm{i}\hbar\,\varepsilon_{pr}\left(\hat{c}^{\dagger}\,\mathrm{e}^{-\mathrm{i}\,\delta t}-\hat{c}\,\mathrm{e}^{\mathrm{i}\,\delta t}\right).\end{aligned}\tag{1}$$

Here, $\hat{Q}_i$ and $\hat{P}_i$ represent two mechanical oscillators' position and momentum operators; $\hat{P}_i^2+\hat{Q}_i^2$ represent the energy of independent oscillators; $\hat{Q}_i^2$ is the energy of the intraspecies oscillator; $\hat{Q}_i\hat{Q}_j$ is the energy of the interspecies oscillator in the first term. The second term represents the nonlinear COMS interactions between DBEC and cavity field with the optomechanical coupling strength ξ_i; $\Delta_c^{'}=\omega_c^{'}-\omega_{pu}$ is the effective optical detuning between COMS and pump laser field, and $\Delta=\omega_{pr}-\omega_{pu}$ is the detuning between probe laser field and external pump laser field. The second line of (1) describes the energy of the cavity field, the strong pump laser field, and the weak probe laser field. The classical light inputs with frequency ω_{pu} and ω_{pr}, and ε_{pu} and ε_{pr} are related to the laser power. The Hamiltonian (1) corresponds to a two-mode COMS; $(\hat{P}_1,\hat{Q}_1)$ is the first mechanical mode, and $(\hat{P}_2,\hat{Q}_2)$ is the second mechanical mode. In this form of the Hamiltonian, the effect of intraspecies

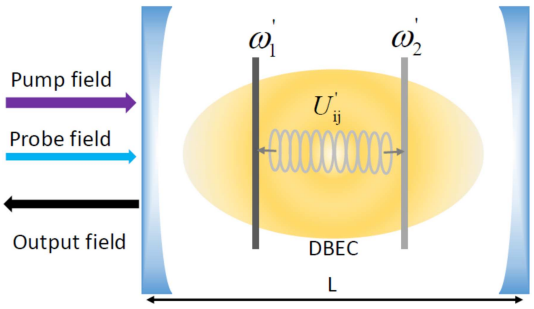

Fig. 1. The hybrid optomechanical system consisting of an ultracold dual-species Bose–Einstein condensate trapped inside an optical cavity. The cavity is driven by a strong pump laser with frequency ω_{pu} and a weak probe laser with frequency ω_{pr}.

oscillator coupling and interspecies oscillator coupling interaction is implied in both frequencies ω_i of the Bogoliubov modes. In (1), the effective resonance frequencies and oscillator couplings are

$$\omega_i=\frac{2\hbar k^2}{m_i}+\frac{2}{L}N_iU_{ii}^{'}+\frac{1}{L}N_jU_{ij}^{'},\tag{2}$$

$$U_{ii}=\frac{2}{L}N_iU_{ii}^{'},\tag{3}$$

$$U_{ij}=\frac{2}{L}\sqrt{N_iN_j}\,U_{ij}^{'},\tag{4}$$

$$\omega_c^{'}=\omega_c+\frac{1}{2}\sum_{i=1,2}N_iU_i.\tag{5}$$

Here m_i is the atomic mass; $k=\frac{2\pi}{\lambda}$ is the wave vector; N_i is the atom number; $U_{ii}^{'}$ is intraspecies oscillator coupling; $U_{ij}^{'}$ is the interspecies oscillator coupling; ω_c is the central frequency of the cavity field ($\omega_c=\frac{n\pi c}{L}$) and $\frac{1}{2}N_iU_i$ is the frequency shift of the empty cavity resonance induced by the condensate of species i; $U_i=g_i/(\omega_c-\omega_i^{'})$, where g_i is the single photon Rabi frequency and $\omega_i^{'}$ is the atomic resonance frequency.

Adding the damping terms, the coupled quantum Langevin equations can be obtained as

$$\begin{aligned}\frac{\mathrm{d}\hat{c}}{\mathrm{d}t}=&-(\kappa+\mathrm{i}\,\Delta_c^{'})\hat{c}-\mathrm{i}\xi_1\hat{Q}_1\hat{c}-\mathrm{i}\xi_2\hat{Q}_2\hat{c}\\&+\varepsilon_{pu}+\varepsilon_{pr}\,\mathrm{e}^{-\mathrm{i}\,\delta t},\end{aligned}\tag{6}$$

$$\frac{\mathrm{d}\hat{Q}_1}{\mathrm{d}t}=\omega_1\hat{P}_1-\gamma_1\hat{Q}_1,\tag{7}$$

$$\frac{\mathrm{d}\hat{Q}_2}{\mathrm{d}t}=\omega_2\hat{P}_2-\gamma_2\hat{Q}_2,\tag{8}$$

$$\frac{\mathrm{d}\hat{P}_1}{\mathrm{d}t}=-(\omega_1+2U_{11})\hat{Q}_1-U_{12}\hat{Q}_2-\xi_1\hat{c}^{\dagger}\hat{c}-\gamma_1\hat{P}_1,\tag{9}$$

$$\frac{\mathrm{d}\hat{P}_2}{\mathrm{d}t}=-(\omega_2+2U_{22})\hat{Q}_2-U_{12}\hat{Q}_1-\xi_2\hat{c}^{\dagger}\hat{c}-\gamma_2\hat{P}_2.\tag{10}$$

The nonlinear (6)–(10) can be linearized via rewriting each mean value of the Heisenberg operator as its steady state value plus an additional perturbation correction, i.e., $\langle c\rangle = c_0+\delta c$, $\langle Q_i\rangle = Q_{i0}+\Delta Q_i$ and $\langle P_i\rangle = P_{i0}+\Delta P_i$. The steady-state solution of the system can be obtained as

$$c_0 = \frac{\varepsilon_{pu}}{\sqrt{\kappa^2+\Delta^2}}, \tag{11}$$

$$Q_{10} = -\frac{\xi_1|c_0|^2+U_{12}Q_{20}}{\omega_1+2U_{11}+\frac{\gamma_1^2}{\omega_1}}, \tag{12}$$

$$Q_{20} = -\frac{\xi_2|c_0|^2+U_{12}Q_{10}}{\omega_2+2U_{22}+\frac{\gamma_2^2}{\omega_2}} \tag{13}$$

with $\Delta = \Delta_c^{'}+\xi_1Q_{10}+\xi_2Q_{20}$ as the effective detuning. Note that c_0, Q_{10} and Q_{20} are the static solution of the intracavity field and the DBEC displacement, respectively. Next, we consider the perturbation made by the probe field — the linearized equations can be written as

$$\frac{\mathrm{d}\delta c}{\mathrm{d}t} = -(\mathrm{i}\Delta+\kappa)\delta c - \mathrm{i}\xi_1(c_0\delta Q_1+\delta c\delta Q_1) - \mathrm{i}\xi_2\big(c_0\delta Q_2+\delta c\delta Q_2\big)+\varepsilon_{pr}\mathrm{e}^{-\mathrm{i}\delta t}, \tag{14}$$

$$\frac{\mathrm{d}\delta Q_1}{\mathrm{d}t} = \omega_1\delta P_1-\gamma_1\delta Q_1, \tag{15}$$

$$\frac{\mathrm{d}\delta P_1}{\mathrm{d}t} = -(\omega_1+2U_{11})\delta Q_1-U_{12}\delta Q_2 - \xi_1\big(c_0^*\delta c+c_0\delta c^*+\delta c\delta c^*\big)-\gamma_1\delta P_1, \tag{16}$$

$$\frac{\mathrm{d}\delta Q_2}{\mathrm{d}t} = \omega_2\delta P_2-\gamma_2\delta Q_2, \tag{17}$$

$$\frac{\mathrm{d}\delta P_2}{\mathrm{d}t} = -(\omega_2+2U_{22})\delta Q_2-U_{12}\delta Q_1 - \xi_2\big(c_0^*\delta c+c_0\delta c^*+\delta c\delta c^*\big)-\gamma_2\delta P_2. \tag{18}$$

Considering SS but ignoring the HS, the perturbation of (14)–(18) can be written as

$$\delta c = c_1^-\mathrm{e}^{-\mathrm{i}\delta t}+c_1^+\mathrm{e}^{\mathrm{i}\delta t}+c_2^-\mathrm{e}^{-2\mathrm{i}\delta t}+c_2^+\mathrm{e}^{2\mathrm{i}\delta t}, \tag{19}$$

$$\delta Q_1 = Q_{11}^-\mathrm{e}^{-\mathrm{i}\delta t}+Q_{11}^+\mathrm{e}^{\mathrm{i}\delta t}+Q_{12}^-\mathrm{e}^{-2\mathrm{i}\delta t}+Q_{12}^+\mathrm{e}^{2\mathrm{i}\delta t}, \tag{20}$$

$$\delta P_1 = P_{11}^-\mathrm{e}^{-\mathrm{i}\delta t}+P_{11}^+\mathrm{e}^{\mathrm{i}\delta t}+P_{12}^-\mathrm{e}^{-2\mathrm{i}\delta t}+P_{12}^+\mathrm{e}^{2\mathrm{i}\delta t}, \tag{21}$$

$$\delta Q_2 = Q_{21}^-\mathrm{e}^{-\mathrm{i}\delta t}+Q_{21}^+\mathrm{e}^{\mathrm{i}\delta t}+Q_{22}^-\mathrm{e}^{-2\mathrm{i}\delta t}+Q_{22}^+\mathrm{e}^{2\mathrm{i}\delta t}, \tag{22}$$

$$\delta P_2 = P_{21}^-\mathrm{e}^{-\mathrm{i}\delta t}+P_{21}^+\mathrm{e}^{\mathrm{i}\delta t}+P_{22}^-\mathrm{e}^{-2\mathrm{i}\delta t}+P_{22}^+\mathrm{e}^{2\mathrm{i}\delta t}. \tag{23}$$

These parameters can be obtained by substituting (19)–(23) into (14)–(18) and comparing the coefficients of the same order. We can obtain the first-order sideband equations as

$$(\kappa+\mathrm{i}\Delta-\mathrm{i}\delta)c_1^- = -\mathrm{i}\xi_1c_0Q_{11}^- - \mathrm{i}\xi_2c_0Q_{21}^-+\varepsilon_{pr}, \tag{24}$$

$$(\kappa+\mathrm{i}\Delta+\mathrm{i}\delta)c_1^+ = -\mathrm{i}\xi_1c_0Q_{11}^+ - \mathrm{i}\xi_2c_0Q_{21}^+, \tag{25}$$

$$-\mathrm{i}\delta Q_{11}^- = \omega_1P_{11}^- - \gamma_1Q_{11}^-, \tag{26}$$

$$\mathrm{i}\delta Q_{11}^+ = \omega_1P_{11}^+ - \gamma_1Q_{11}^+, \tag{27}$$

$$-\mathrm{i}\delta P_{11}^- = -(\omega_1+2U_{11})Q_{11}^- - U_{12}Q_{21}^- - \gamma_1P_{11}^- - \xi_1\big(c_0^*c_1^-+c_0c_1^{+*}\big), \tag{28}$$

$$\mathrm{i}\delta P_{11}^+ = -(\omega_1+2U_{11})Q_{11}^+ - U_{12}Q_{21}^+ - \gamma_1P_{11}^+ - \xi_1\big(c_0^*c_1^++c_0c_1^{-*}\big), \tag{29}$$

$$-\mathrm{i}\delta Q_{21}^- = \omega_2P_{21}^- - \gamma_2Q_{21}^-, \tag{30}$$

$$\mathrm{i}\delta Q_{21}^+ = \omega_2P_{21}^+ - \gamma_2Q_{21}^+, \tag{31}$$

$$-\mathrm{i}\delta P_{21}^- = -(\omega_2+2U_{22})Q_{21}^- - U_{12}Q_{11}^- - \gamma_2P_{21}^- - \xi_2\big(c_0^*c_1^-+c_0c_1^{+*}\big), \tag{32}$$

$$\mathrm{i}\delta P_{21}^+ = -(\omega_2+2U_{22})Q_{21}^+ - U_{12}Q_{11}^+ - \gamma_2P_{21}^+ - \xi_2\big(c_0^*c_1^++c_0c_1^{-*}\big). \tag{33}$$

Based on the steady-state solutions (11)–(13), we find the first-order sideband analytical expressions

$$c_1^- = \frac{\big(1+\mathrm{i}f_1(\delta)|c_0|^2\big)\varepsilon_{pr}}{\kappa+\mathrm{i}\Delta-\mathrm{i}\delta-2\Delta f_1(\delta)|c_0|^2}, \tag{34}$$

$$Q_{11}^- = \frac{A_1(\delta)c_0^*\varepsilon_{pr}}{\kappa+\mathrm{i}\Delta-\mathrm{i}\delta-2\Delta f_1(\delta)|c_0|^2}, \tag{35}$$

$$Q_{21}^- = \frac{A_2(\delta)c_0^*\varepsilon_{pr}}{\kappa+\mathrm{i}\Delta-\mathrm{i}\delta-2\Delta f_1(\delta)|c_0|^2}, \tag{36}$$

with

$$\lambda_1(\delta) = \frac{\omega_1}{\omega_1\big(\omega_1+2U_{11}\big)+\big(\gamma_1-\mathrm{i}\delta\big)^2}, \tag{37}$$

$$\lambda_2(\delta) = \frac{\omega_2}{\omega_2\big(\omega_2+2U_{22}\big)+\big(\gamma_2-\mathrm{i}\delta\big)^2}, \tag{38}$$

$$A_1(\delta) = \frac{-\lambda_1(\delta)\xi_1+\xi_2U_{12}\lambda_1(\delta)\lambda_2(\delta)}{1-\lambda_1(\delta)\lambda_2(\delta)U_{12}^2}, \tag{39}$$

$$A_2(\delta) = \frac{-\lambda_2(\delta)\xi_2+\xi_1U_{12}\lambda_1(\delta)\lambda_2(\delta)}{1-\lambda_1(\delta)\lambda_2(\delta)U_{12}^2}, \tag{40}$$

$$f_1(\delta) = \frac{\xi_1^2\lambda_1(\delta)+\xi_2^2\lambda_2(\delta)-2\xi_1\xi_2U_{12}\lambda_1(\delta)\lambda_2(\delta)}{\big(\kappa-\mathrm{i}\Delta-\mathrm{i}\delta\big)\big(1-\lambda_1(\delta)\lambda_2(\delta)U_{12}^2\big)}. \tag{41}$$

Then, we can get the SS equations as

$$(\kappa+\mathrm{i}\Delta-2\mathrm{i}\delta)c_2^- = -\mathrm{i}\xi_1(c_0Q_{12}^-+c_1^-Q_{11}^-) - \mathrm{i}\xi_2(c_0Q_{22}^-+c_1^-Q_{21}^-), \tag{42}$$

$$(\kappa+\mathrm{i}\Delta+2\mathrm{i}\delta)c_2^+ = -\mathrm{i}\xi_1\big(c_0Q_{12}^++c_1^+Q_{11}^+\big) - \mathrm{i}\xi_2\big(c_0Q_{22}^++c_1^+Q_{21}^+\big), \tag{43}$$

$$-2\mathrm{i}\delta Q_{12}^{-}=\omega_1 P_{12}^{-}-\gamma_1 Q_{12}^{-}, \tag{44}$$

$$2\mathrm{i}\delta Q_{12}^{+}=\omega_1 P_{12}^{+}-\gamma_1 Q_{12}^{+}, \tag{45}$$

$$-2\mathrm{i}\delta P_{12}^{-}=-(\omega_1+2U_{11})Q_{12}^{-}-\gamma_1 P_{12}^{-}-U_{12}Q_{22}^{-} -\xi_1\big(c_0^{*}c_2^{-}+c_0c_2^{+*}+c_1^{-}c_1^{+*}\big), \tag{46}$$

$$2\mathrm{i}\delta P_{12}^{+}=-(\omega_1+2U_{11})Q_{12}^{+}-\gamma_1 P_{12}^{+}-U_{12}Q_{22}^{+} -\xi_1\big(c_0^{*}c_2^{+}+c_0c_2^{-*}+c_1^{+}c_1^{-*}\big), \tag{47}$$

$$-2\mathrm{i}\delta Q_{22}^{-}=\omega_2 P_{22}^{-}-\gamma_2 Q_{22}^{-}, \tag{48}$$

$$2\mathrm{i}\delta Q_{22}^{+}=\omega_2 P_{22}^{+}-\gamma_2 Q_{22}^{+}, \tag{49}$$

$$-2\mathrm{i}\delta P_{22}^{-}=-(\omega_2+2U_{22})Q_{22}^{-}-\gamma_2 P_{22}^{-}-U_{12}Q_{12}^{-} -\xi_2\big(c_0^{*}c_2^{-}+c_0c_2^{+*}+c_1^{-}c_1^{+*}\big), \tag{50}$$

$$2\mathrm{i}\delta P_{22}^{+}=-(\omega_2+2U_{22})Q_{22}^{+}-\gamma_2 P_{22}^{+}-U_{12}Q_{12}^{+} -\xi_2\big(c_0^{*}c_2^{+}+c_0c_2^{-*}+c_1^{+}c_1^{-*}\big). \tag{51}$$

We find the SS analytical expressions and obtain c_2^{-} as follows

$$c_2^{-}=\frac{-\mathrm{i}f_1(2\delta)c_0\big(\mathrm{i}\xi_1Q_{11}^{-}+\mathrm{i}\xi_2Q_{21}^{-}\big)^2+\big((2\Delta-\delta)f_1(2\delta)-1\big)\big(\mathrm{i}\xi_1c_1^{-}Q_{11}^{-}-\mathrm{i}\xi_2c_1^{-}Q_{21}^{-}\big)}{\kappa+\mathrm{i}\Delta-2\mathrm{i}\delta+2\Delta f_1(2\delta)\big(\kappa-\mathrm{i}\Delta-\mathrm{i}\delta\big)}, \tag{52}$$

with

$$\lambda_1(2\delta)=\frac{\omega_1}{\omega_1\big(\omega_1+2U_{11}\big)+\big(\gamma_1-\mathrm{i}2\delta\big)^2}, \tag{53}$$

$$\lambda_2(2\delta)=\frac{\omega_2}{\omega_2\big(\omega_2+2U_{22}\big)+\big(\gamma_2-\mathrm{i}2\delta\big)^2}, \tag{54}$$

$$A_1(2\delta)=\frac{-\lambda_1(2\delta)\xi_1+\xi_2U_{12}\lambda_1(2\delta)\lambda_2(2\delta)}{1-\lambda_1(2\delta)\lambda_2(2\delta)U_{12}^2}, \tag{55}$$

$$A_2(2\delta)=\frac{-\lambda_2(2\delta)\xi_2+\xi_1U_{12}\lambda_1(2\delta)\lambda_2(2\delta)}{1-\lambda_1(2\delta)\lambda_2(2\delta)U_{12}^2}, \tag{56}$$

$$f_1(2\delta)=\frac{\xi_1^2|c_0|^2A_1(2\delta)+\xi_2^2|c_0|^2A_2(2\delta)}{\big(\kappa-\mathrm{i}\Delta-2\mathrm{i}\delta\big)\big(\kappa-\mathrm{i}\Delta-\mathrm{i}\delta\big)}. \tag{57}$$

Next, we use the input-output relation

$$c_{\mathrm{out}}(t)=c_{\mathrm{in}}(t)-\sqrt{2\kappa}\,c(t), \tag{58}$$

where c_{in} and c_{out} are the input and output operators. For our hybrid COMS, we can obtain the output field

$$\begin{aligned}c_{\mathrm{out}}(t)=&(\varepsilon_{pu}/\sqrt{2\kappa}-\sqrt{2\kappa}\,c_0)\,\mathrm{e}^{-\mathrm{i}\omega_{pu}t}\\&+(\varepsilon_{pr}/\sqrt{2\kappa}-\sqrt{2\kappa}\,c_1^{-})\,\mathrm{e}^{-\mathrm{i}(\omega_{pu}+\delta)t}\\&-\sqrt{2\kappa}\,c_1^{+}\,\mathrm{e}^{-\mathrm{i}(\omega_{pu}-\delta)t}-\sqrt{2\kappa}\,c_2^{-}\,\mathrm{e}^{-\mathrm{i}(\omega_{pu}+2\delta)t}\\&-\sqrt{2\kappa}\,c_2^{+}\,\mathrm{e}^{-\mathrm{i}(\omega_{pu}-2\delta)t},\end{aligned} \tag{59}$$

where $c_{\mathrm{out}}(t)$ is the output field operator in the original frame.

The terms $(\varepsilon_{pu}/\sqrt{2\kappa}-\sqrt{2}\,\kappa c_0)\,\mathrm{e}^{-\mathrm{i}\omega_{pu}t}$ and $(\varepsilon_{pr}/\sqrt{2\kappa}-\sqrt{2\kappa}c_1^{-})\,\mathrm{e}^{-\mathrm{i}(\omega_{pu}+\delta)t}$ describe the output fields with the frequencies of the driven field ω_{pu} and the probe field ω_{pr}, respectively. The transmission of the probe field is defined as $t_p=\frac{\varepsilon_{pr}/\sqrt{2\kappa}-\sqrt{2\kappa}\,c_1^{-}}{\varepsilon_{pr}/\sqrt{2\kappa}}$, with the optical transmission strength

$$|t_p|^2=\left|\frac{\varepsilon_{pr}/\sqrt{2\kappa}-\sqrt{2\kappa}\,c_1^{-}}{\varepsilon_{pr}/\sqrt{2\kappa}}\right|^2. \tag{60}$$

The term $\sqrt{2\kappa}c_1^{+}\,\mathrm{e}^{-\mathrm{i}(\omega_{pu}-\delta)t}$ describes the Stokes process at the frequency $2\omega_{pu}-\omega_{pr}$ in (59). The terms $-\sqrt{2\kappa}\,c_2^{-}\,\mathrm{e}^{-\mathrm{i}(\omega_{pu}+2\delta)t}$ and $-\sqrt{2\kappa}\,c_2^{+}\,\mathrm{e}^{-\mathrm{i}(\omega_{pu}-2\Delta)t}$ individually describe the sideband process of upper and lower SS with frequency $2\omega_{pr}-\omega_{pu}$ and $3\omega_{pu}-\omega_{pr}$.

The amplitude of the input probe light is ε_{pr}, while the amplitude of the output field with the second-order sideband $\sqrt{2\kappa}c_2^{-}\,\mathrm{e}^{-\mathrm{i}(\omega_{pu}+2\delta)t}$. In order to analyze the upper SS in our system, we introduce the dimensionless quantity

$$\eta_s=\left|\frac{-\sqrt{2\kappa}\,c_2^{-}}{\varepsilon_{pr}}\right| \tag{61}$$

to describe the efficiency of the upper SS process.

3. Results and discussion

In order to better understand the transmission intensity of the probe field and the dimensionless amplitude of SS in the DBEC optomechanical system, we choose the realistic parameters of the hybrid COMS as follows [19, 53]. We consider $N_{1,2}=1.2\times10^5$ DBEC inside an optical cavity with length $L=178$ μm, driven by single mode external field with laser wavelength $\lambda=500$ nm and the intra-cavity optical mode with decay rate κ. Further, the parameters of stable (^{87}Rb–^{41}K) DBEC are $m_1=87\mu_0$, $m_2=41\mu_0$, $\mu_0\simeq1.7\times10^{-27}$ kg; the frequency shifts are $\omega_1=91$ kHz $=7\kappa$ and $\omega_2=117$ kHz $=9\kappa$ with damping $\gamma_1=\gamma_2=0.001\kappa$. The results are based on some conditions; the first one is the resolved sideband condition $\omega_i\gg\kappa$ to ensure that we can distinguish the normal mode splitting; the second one is that the cavity is driven by the red detuned cavity field $\Delta=\frac{1}{2}(\omega_1+\omega_2)=\bar{\omega}$.

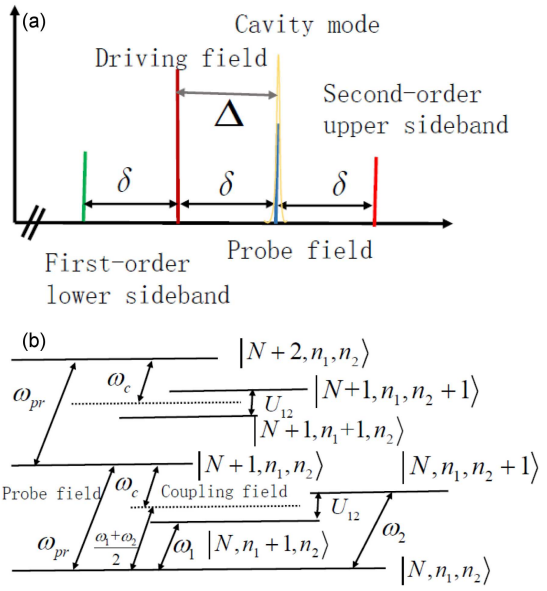

Fig. 2. (a) Frequency spectrogram of transmission spectra in the present system in DBEC optomechanical system. There is the upper SS generation at the frequency 2Δ in a frame rotating at ω_{pu}. (b) Schematic of the energy-level diagram in the cavity optomechanical system, where $|N\rangle$, $|n_1\rangle$ and $|n_2\rangle$ denote the number states of the cavity photon, and two effective movable mirrors phonons, respectively.

Physically, we can explain the possible processes in our system using a level diagram as shown in Fig. 2. From the frequency spectrogram in Fig. 2a, it can be seen that the output field of the frequencies of the probe field ω_{pr} and the upper SS generation has the frequency of $\omega_{pu}+2\Delta$. In the energy-level diagram in Fig. 2b, $|N,n_1,n_2\rangle \leftrightarrow |N+1,n_1,n_2\rangle$ and $|N+1,n_1,n_2\rangle \leftrightarrow |N+2,n_1,n_2\rangle$ transitions change the cavity field, $|N+1,n_1,n_2\rangle \leftrightarrow |N,n_1+1,n_2\rangle$ and $|N+1,n_1,n_2\rangle \leftrightarrow |N,n_1,n_2+1\rangle$ transitions are caused by the radiation pressure coupling, and $|N,n_1+1,n_2\rangle \leftrightarrow |N,n_1,n_2+1\rangle$ transition is induced by the effective intraspecies interaction strengths. Such a nonlinear output field is generated mainly by the combination of the four-wave mixing process $|N,n_1,n_2\rangle \rightarrow |N+1,n_1,n_2\rangle \rightarrow |N+2,n_1,n_2\rangle \rightarrow |N+1,n_1+1,n_2\rangle \rightarrow |N,n_1,n_2\rangle$ and the anti-Stokes process $|N,n_1,n_2\rangle \rightarrow |N+1,n_1,n_2\rangle \rightarrow |N+1,n_1+1,n_2\rangle \rightarrow |N,n_1,n_2\rangle$ mediated by $|N,n_1+1,n_2\rangle$ and $|N,n_1,n_2+1\rangle$, as depicted in Fig. 2b. The destructive interference has two paths when the frequencies of the two resonances $\omega_1 \neq \omega_2$. The coupling between the oscillator resonance frequency ω_1 and ω_2 not only adds a new level but also breaks down the symmetry of the OMIT interference, as shown in Fig. 2, which means that the single OMIT window can split into two OMIT windows. Due to the radiation pressure, the coherent-induced splitting of OMIT of our COMS is similar to driving a hyperfine transition in an atomic Λ-type three-level system [58].

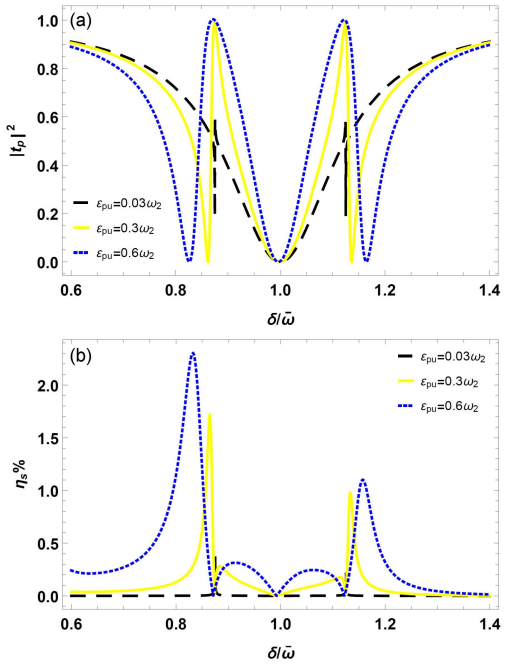

Fig. 3. (a) the transmission intensity $|t_p|^2$ and (b) the dimensionless amplitude of the second-order sideband η_s vary with $\Delta/\bar{\omega}$ for different control field intensities: (i) $\varepsilon_{pu}=0.03\omega_2$ (the black dotted line), (ii) $\varepsilon_{pu}=0.3\omega_2$ (the yellow line), (iii) $\varepsilon_{pu}=0.6\omega_2$ (the blue dot line). The other parameters are: $N_{1,2}=1.2\times10^5$, $\omega_1=2\pi\times91$ kHz, $\omega_2=2\pi\times117$ kHz, $\kappa=2\pi\times1.3\times10^4$ Hz, and $\gamma_1=\gamma_2=0.001\kappa$.

In order to modulate DBEC in the hybrid COMS, we analyze the influences of the transmission intensity and the dimensionless amplitude of SS on the COMS parameters, including the control field intensities, the effective detuning, the effective coupling strength of the optical field with the Bogoliubov mode of the collective oscillation of DBEC, and interspecies and intraspecies interaction strengths in Figs. 3–8.

First, we show the transmission intensity $|t_p|^2$ and the dimensionless amplitude η_s of SS as function of the normalized detuning $\Delta/\bar{\omega}$ in the DBEC optomechanical system for different control field intensities: (i) $\varepsilon_{pu}=0.03\omega_2$ (the black dotted line), (ii) $\varepsilon_{pu}=0.3\omega_2$ (the yellow line), (iii) $\varepsilon_{pu}=0.6\omega_2$ (the blue dotted line) in Fig. 3. Like the typical COMS, there are two obvious phenomena, one is that the efficiency of the transmission intensity generation experiences an evident enhancement with the increase of the control field intensities, another one is that the width of transparency window is further and further apart with the increase of the control field intensity in Fig. 3a. Moreover, we can also clearly see that the dimensionless amplitude of the SS generation experiences an obvious enhancement with the increase of the control field intensities; the asymmetric splitting effect of the SS peak appears

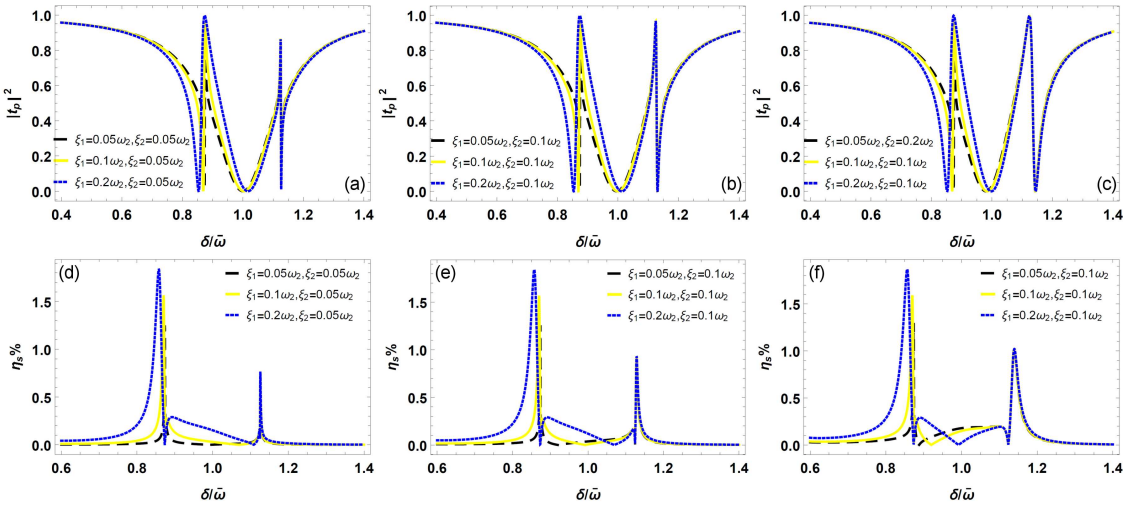

Fig. 4. Calculation results of the transmission intensity $|t_p|^2$ and the dimensionless amplitude of the second-order sideband η_s vary with $\Delta/\bar{\omega}$ for different effective coupling between the Bogoliubov mode of the collective oscillation of DBEC and optical mode: (i) $\xi_1 = 0.05\omega_2$ (black dashed line), (ii) $\xi_1 = 0.1\omega_2$ (yellow line), (iii) $\xi_1 = 0.2\omega_2$ (blue dashed line). The other parameters are the same as those of Fig. 3.

in Fig. 3b. The physical effect can be explained by the fact that the number of photons in the cavity increases as the strength of the control field increases, and the SS effect will be induced due to the strong photon pressure on the resonator enhancing the amplitude of the Bogoliubov mode of the collective oscillation of DBEC. As the power of the control field becomes larger, SS experiences the conversion from a weakness to an enhancement. As seen from the results obtained in Fig. 3, the transmission intensity and the dimensionless amplitude of the SS generation can be effectively controlled by adjusting the control field intensities.

Second, in order to see the effective coupling strength of the optical field with the Bogoliubov mode on the transmission intensity $|t_p|^2$ and the dimensionless amplitude η_s of SS, we plot the transmission intensity and the dimensionless amplitude as a function of the probe-pump detuning $\Delta/\bar{\omega}$ for different effective coupling strengths: (i) $\xi_2 = 0.05\omega_2$ (in panels (a) and (d)), (ii) $\xi_2 = 0.1\omega_2$ (in panels (b) and (e)), (iii) $\xi_2 = 0.2\omega_2$ (in panels (c)and (f)) in Fig. 4. There are three obvious phenomena. First of all, it was discovered that when the effective coupling between the Bogoliubov mode of DBEC and optical mode are equal, i.e., (i) $\xi_1 = \xi_2 = 0.05\omega_2$ (Fig. 4a black dashed line), (ii) $\xi_1 = \xi_2 = 0.1\omega_2$ (Fig. 4b yellow line), and (iii) $\xi_1 = \xi_2 = 0.2\omega_2$ (Fig. 4c blue dashed line), the transmission intensity has two symmetrical OMIT windows, the splitting effect of the SS peak appears, and the peak on the left is higher than the peak on the right. Secondly, when the effective coupling between the Bogoliubov mode of DBEC and optical mode are not equal, i.e., (i) $\xi_1 = 0.05\omega_2$ (black dashed line), (ii) $\xi_1 = 0.1\omega_2$ (yellow line), and (iii) $\xi_1 = 0.2\omega_2$ (blue dashed line) at the same coupling intensity $\xi_2 = 0.05\omega_2$ in panels Fig. 4a and Fig. 4d, it can be clearly seen that symmetrical two OMIT windows become asymmetrical, the splitting effect of the SS peak appears on the left, and a single resonance peak appears on the right. Thirdly, as the effective coupling strength increases, i.e., $\xi_2 = 0.1\omega_2$ in Fig. 4b and e and $\xi_2 = 0.2\omega_2$ in Fig. 4c and f, the splitting effect of the SS peak appears on the left and right. Figure 4 shows that the transmission intensity and the SS effects can be achieved in such COMS as expected. The nature of this phenomenon can be understood as follows — concurrently with the increase of the effective coupling between the Bogoliubov mode of DBEC and the optical mode ξ_1 and ξ_2, the photon density in the cavity increases greatly, which will induce strong photon pressure on the Bogoliubov mode of DBEC. As a result, controlling the effective coupling strength allows us to change the transmission intensity $|t_p|^2$ and the dimensionless amplitude η_s of SS.

Moreover, effective detuning Δ is an important parameter used for modulating the transmission intensity $|t_p|^2$ and the dimensionless amplitude η_s of SS. Considering $\Delta = \omega_1$, $\Delta = \bar{\omega}$, and $\Delta = \omega_2$ in the calculation, we have plotted the transmission intensity $|t_p|^2$ (see Fig. 5a–c) and the dimensionless amplitude η_s of SS (see Fig. 5d–f) varying with the effective detuning $\Delta/\bar{\omega}$. There are two very significant phenomena in Fig. 5 that will be slightly different from those above for $\Delta = \bar{\omega}$. As is shown in Fig. 5b and e, when the effective detuning $\Delta = \bar{\omega}$, the transmission intensity $|t_p|^2$, and the dimensionless amplitude η_s of the SS generation present a symmetrical profile with two splitting peaks. However, when $\Delta = \omega_1$ and $\Delta = \omega_2$ are tuned not to be equal with $\bar{\omega}$, the symmetrical two OMIT windows become asymmetrical, which can

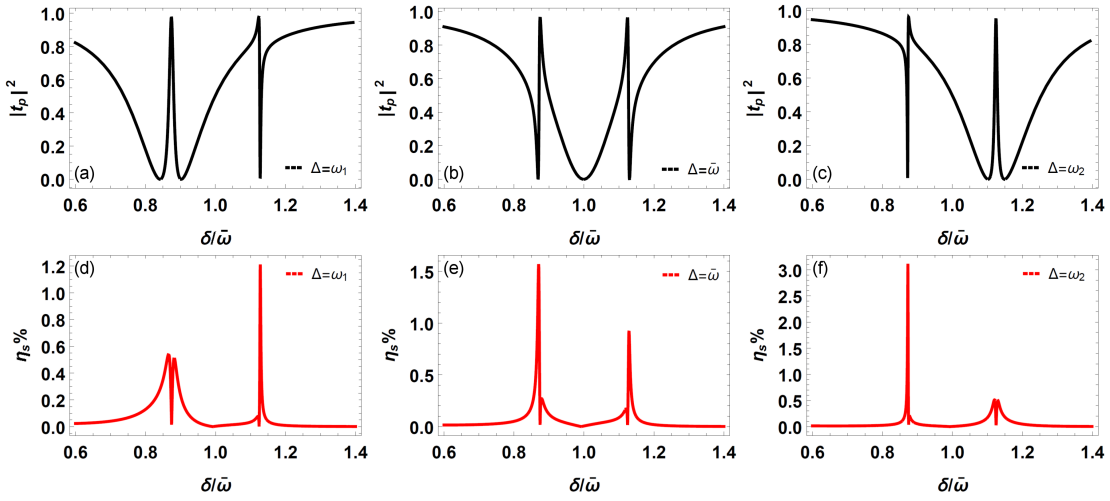

Fig. 5. Calculation results of the transmission intensity $|t_p|^2$ and the dimensionless amplitude of the second-order sideband η_s vary with $\Delta/\bar{\omega}$ for the three different effective atom-pump detuning: (i) $\Delta = \omega_1$, (ii) $\Delta = \bar{\omega}$, (iii) $\Delta = \omega_2$. The other parameters are the same as those of Fig. 3.

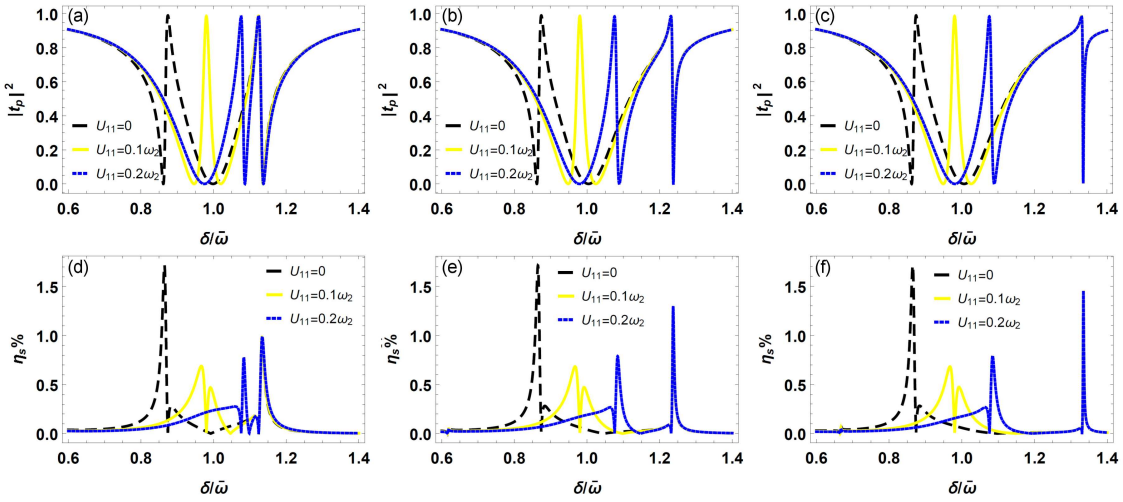

Fig. 6. Calculation results of the transmission intensity $|t_p|^2$ and the dimensionless amplitude of the second-order sideband η_s vary with $\Delta/\bar{\omega}$ for different interspecies oscillator couplings: (i) $U_{11} = 0$ (black dashed line), (ii) $U_{11} = 0.1\omega_2$ (yellow line), (iii) $U_{11} = 0.2\omega_2$ (blue dashed line); meanwhile in (a, d) $U_{22} = 0$, in (b, e) $U_{22} = 0.1\omega_2$, in (c, f) $U_{22} = 0.2\omega_2$. The other parameters are the same as those of Fig. 3.

be seen in Fig. 5a and c. When $\Delta = \omega_1$ is tuned to be less than $\bar{\omega}$, the right peak of the effective amplitude η_s profile is enhanced remarkably, and the symmetry of two splitting peaks is broken, which can be seen in Fig. 5d. When $\Delta = \omega_2$ is larger than $\bar{\omega}$, the left peak of the dimensionless amplitude η_s profile is amplified significantly, and the symmetry of two splitting peaks is also broken, which can be seen in Fig. 5f. Thus, adjusting the effective detuning will affect the transmission intensity of probe field and the dimensionless amplitude of SS.

Furthermore, the transmission intensity $|t_p|^2$ and the dimensionless amplitude η_s of SS as a function of the normalized detuning $\Delta/\bar{\omega}$ for different intraspecies oscillator couplings: $U_{11} = 0$ (black dashed line), $U_{11} = 0.1\omega_2$ (yellow line), $U_{11} = 0.2\omega_2$ (blue dashed line), and (a, d) $U_{22} = 0$, (b, e) $U_{22} = 0.1\omega_2$, (c, f) $U_{22} = 0.2\omega_2$. This is shown in Fig. 6. There are two obvious phenomena observed. First one is when the interspecies oscillator coupling U_{22} is fixed, while U_{11} varies ($U_{11} = \{0, 0.1\omega_2, 0.2\omega_2\}$). By comparing the corresponding three different color curves in panels Fig. 6a and d, it can be concluded that with the increase of the interspecies oscillator coupling strength U_{11}, the width between the two peaks about OMIT and the amplitude of SS become narrower and narrower. The one is when the interspecies oscillator coupling U_{11} is fixed, while U_{22} varies (for example, the blue dashed line in Fig. 6). By comparing the blue dashed lines

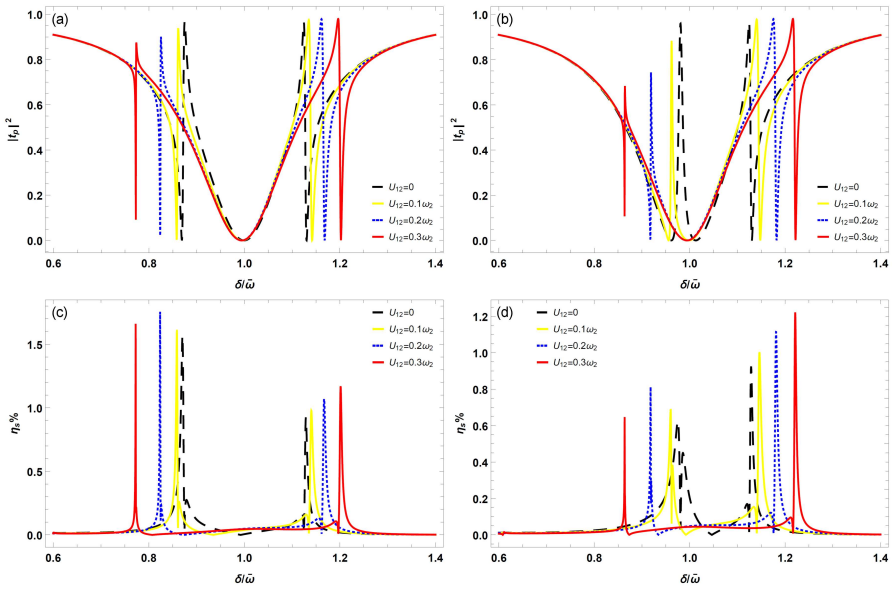

Fig. 7. Calculation results of the transmission intensity $|t_p|^2$ and the dimensionless amplitude of the second-order sideband η_s vary with $\Delta/\bar{\omega}$ for different interspecies oscillator coupling: (i) $U_{12} = 0\omega_2$ (black dashed line), (ii) $U_{12} = 0.1\omega_2$ (yellow line), (iii) $U_{12} = 0.2\omega_2$ (blue dashed line) and (iv) $U_{12} = 0.3\omega_2$ (red line), meanwhile, in panels (a) and (c), we use $U_{11} = 0$; in panels (b) and (d), we use $U_{11} = 0.1\omega_2$. The other parameters are the same as those of Fig. 3.

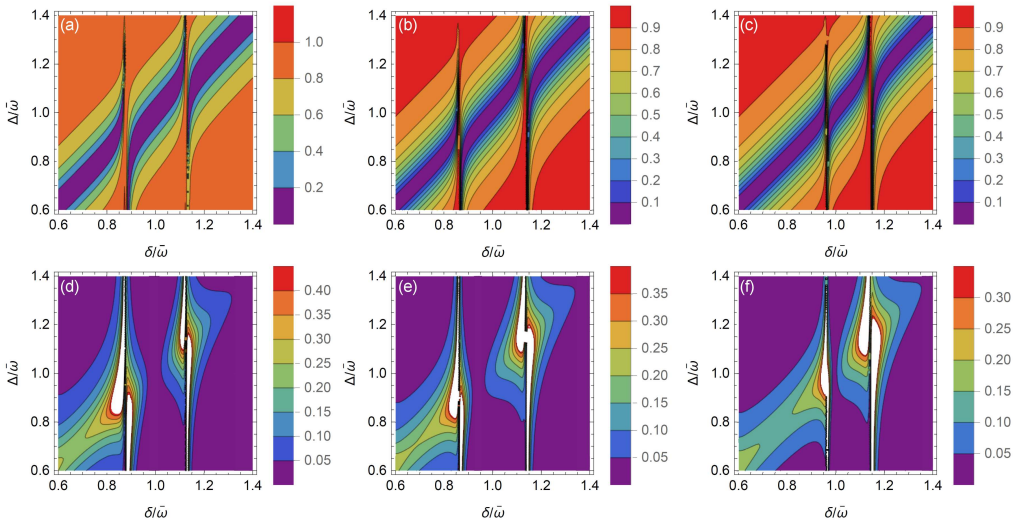

Fig. 8. Contour maps of the transmission intensity $|t_p|^2$ including (a)–(c) and the dimensionless amplitude of the second-order sideband η_s including (d)–(f) as a function of the effective atom-pump detuning $\Delta/\bar{\omega}$ and the control field detuning $\Delta/\bar{\omega}$ with different interspecies oscillator coupling and the interaction coupling strengths. (i) $U_{11} = 0$ and $U_{12} = 0$ (a), (d), (ii) $U_{11} = 0\omega_2$ and $U_{12} = 0.1\omega_2$ (b), (e), and (iii) $U_{11} = 0.1\omega_2$ and $U_{12} = 0.1\omega_2$ (c), (f). The other parameters are the same as those of Fig. 3.

in Fig. 6a–c and Fig. 6d–f, it can be concluded that with the increase of the interspecies oscillator coupling strength U_{22}, the two peaks about OMIT and the dimensionless amplitude of the SS shift to the right, and at the same time, the width between the two peaks becomes larger and larger. The reason for this can be explained by the coefficient of the analytical expressions for the output transmission intensity and the dimensionless amplitude of SS

$$\lambda_i(\Delta) = \frac{\omega_i}{\omega_i(\omega_i+2U_{ii}) + (\gamma_i - \mathrm{i}\,\Delta)^2} \tag{62}$$

and

$$\lambda_i(2\Delta) = \frac{\omega_i}{\omega_i(\omega_i+2U_{ii}) + (\gamma_i - \mathrm{i}\,2\Delta)^2}, \tag{63}$$

where $i = 1, 2$. As follows from (62)–(63), first of all, in our model we use $\omega_1 < \omega_2$, then notice the expression in the denominator $\omega_1(\omega_1 + 2U_{11})$ and

$\omega_2(\omega_2 + 2U_{22})$, by controlling the interspecies oscillator coupling, the frequency difference between $\omega_1(\omega_1 + 2U_{11})$ and $\omega_2(\omega_2 + 2U_{22})$ break down the symmetry of the OMIT interference and the dimensionless amplitude of SS, and then symmetrical windows become asymmetrical. These results confirm that the interspecies oscillator coupling plays an important role in the transmission intensity and the dimensionless amplitude of the SS generation.

In addition, the transmission intensity $|t_p|^2$ and the dimensionless amplitude η_s of SS as a function of the normalized detuning $\Delta/\bar{\omega}$ for different interspecies oscillator coupling: (i) $U_{12} = 0$ (black dashed line), (ii) $U_{12} = 0.1\omega_2$ (yellow line), (iii) $U_{12} = 0.2\omega_2$ (blue dashed line), and (iv) $U_{12} = 0.3\omega_2$ (red line) in the presence of the intraspecies interaction, are shown in Fig. 7. There are two very significant phenomena shown in Fig. 7. First one is that when there are no interspecies and intraspecies interactions in Fig. 7a and c (the black dashed line), it can be clearly seen that symmetrical two OMIT windows and the SS generation present a profile with two splitting peaks. While in the presence of the intraspecies interaction, but in the absence of the interspecies interaction, as shown in Fig. 7a and c (the yellow line, the blue dashed line, and the red line), it can clearly be seen that symmetrical two OMIT windows become asymmetrical, the splitting effect of the SS peak appears on the right, and a single resonance peak appears on the left with increase the intraspecies interaction. The second one is that when in the presence of the intraspecies interaction and the interspecies interaction, as shown in Fig. 7b and d, the two peaks about OMIT and the dimensionless amplitude of the SS shift to the right, and at the same time, the width between the two peaks becomes larger and larger.

Finally, in order to see the effective detuning and the effect of interspecies and intraspecies interaction strengths on the transmission intensity $|t_p|^2$ and the dimensionless amplitude η_s of SS, we plot the transmission intensity of probe field $|t_p|^2$ and the dimensionless amplitude η_s of SS varying with probe-pump detuning $\Delta/\bar{\omega}$ and the effective detuning $\Delta/\bar{\omega}$ for three different interspecies and intraspecies interaction values: $U_{11} = 0$ and $U_{12} = 0$ (Fig. 8a, d), $U_{11} = 0\omega_2$ and $U_{12} = 0.1\omega_2$ (Fig. 8b, e), and $U_{11} = 0.1\omega_2$ and $U_{12} = 0.1\omega_2$ (Fig. 8c, f). For the three cases of $|t_p|^2$ (Fig. 8a–c) and η_s (Fig. 8d–f), one can find that the transmission intensity $|t_p|^2$ and the dimensionless amplitude η_s of the SS depends highly on the effective detuning Δ. Moreover, with the interspecies and intraspecies interaction increasing, the local maximums of $|t_p|^2$ and η_s have a giant enhancement at the off-resonance position of the probe-pulsed detuning. Physically, the detuning management of nonlinear response plays an important role in optical nonlinear modulation. This implies that the frequency detuning between the cavity field and control field changes the optical nonlinear strength of COMS and affects the dimensionless amplitude of the SS output. Comparing $|t_p|^2$ in Fig. 8a–c with η_s in Fig. 8d–f, for a fixed probe-pump detuning, the maximums of $|t_p|^2$ and η_s are always located in the extremely narrow frequency ranges, where their corresponding transmission intensities $|t_p|^2$ and the dimensionless amplitude η_s of SS show an asymmetric dip, as shown in Figs. 6 and 7.

4. Conclusions

In conclusion, we have theoretically investigated the efficient generation of the optical SS in a cigar-shaped DBEC inside a single-mode, high-finesse Fabry–Pérot cavity, both mirrors of which are fixed. We show that the hybrid cavity photomechanical system is different, mainly in the optomechanical coupling between the cavity photons and the two fictitious mirrors. We investigate the matter-wave analog of OMIT and the dimensionless amplitude of SS under different parameter regimes. First of all, we show that atomic collisions provide linear couplings between fictitious condensate oscillators, which facilitates the mechanical mixing of DBEC. We derive analytical expressions of the output transmission intensity and the dimensionless amplitude of SS. The numerical results show that the transmission intensity and the dimensionless amplitude of SS can be controlled by the interspecies and intraspecies interaction. Furthermore, the transmission intensity and the dimensionless amplitude of SS can be controlled by the control field intensities, the effective detuning, and the effective coupling strength of the Bogoliubov mode of DBEC and the optical mode. We believe that this new method of SS generation proposed here will be implemented by current experiments in the future.

Acknowledgments

Project supported by the National Natural Science Foundation of Gansu Province, China (Grant No. 20JR5RA509), the Youth Doctor Foundation of Gansu Provincial Department of Education (No. 2022QB-023, 2022QB-019), Teaching Achievement Cultivation Project of Gansu Provincial Department of Education (2022GSJXCGPY-06), the Fundamental Research Funds for the Central Universities, Northwest Minzu University (No. 31920210016, 31920200006), Education and Teaching Reform Project, Northwest Minzu University (No. 2021XJYBJG-206).

References

[1] T.J. Kippenberg, K.J. Vahala, *Science* **321**, 1172 (2008).

[2] S. Ritter, C. Nölleke, C. Hahn, A. Reiserer, A. Neuzner, M. Uphoff, M. Mücke, E. Figueroa, J. Bochmann, G. Rempe, *Nature* **484**, 195 (2012).

[3] M. Aspelmeyer, P. Meystre K. Schwab, *Phys. Today* **65**, 29 (2012).

[4] M. Aspelmeyer, T.J. Kippenberg, F. Marquardt, *Rev. Mod. Phys.* **86**, 1391 (2014).

[5] G.S. Agarwal, S. Huang, *Phys. Rev. A* **81**, 041803 (2010).

[6] S. Huang, G.S. Agarwal, *Phys. Rev. A* **81** 033830 (2010).

[7] A.H. Safavi-Naeini, T.P. Mayer Alegre, J. Chan, M. Eichenfield, M. Winger, Q. Lin, J. T. Hill, D. Chang, O. Painter, *Nature* **472**, 69 (2011).

[8] T.P. Purdy, K.E. Grutter, K. Srinivasan, J.M. Taylor, *Science* **356**, 1265 (2017).

[9] P. Treutlein, D. Hunger, S. Camerer, T.W. Hänsch, J. Reichel, *Phys. Rev. Lett.* **99**, 140403 (2007).

[10] J.D. Teufel, D. Li, M.S. Allman, K. Cicak, A.J. Sirois, J.D. Whittaker, R.W. Simmonds, *Nature* **471**, 204 (2011).

[11] Q. Zheng, Y. Yao, Y. Li, *Phys. Rev. A* **93**, 013848 (2016).

[12] C.G. Liao, R.X. Chen, H. Xie, M.Y. He, X.M. Lin, *Phys. Rev. A* **99**, 033818 (2019).

[13] F. Monifi, J. Zhang, S.K. Özdemir, B. Peng, Y.X. Liu, F. Bo, F. Nori, L. Yang, *Nat. Photon.* **10** 399 (2016).

[14] B. Peng, S.K. Özdemir, W.J. Chen, F. Nori, L. Yang, *Nat. Commun.* **5**, 5082 (2014).

[15] S. Gupta, K.L. Moore, K.W. Murch, D.M. Stamper-Kurn, *Phys. Rev. Lett.* **99**, 213601 (2007).

[16] A.B. Bhattacherjee, *Phys. Rev. A* **80**, 043607 (2009).

[17] R. Kanamoto, P. Meystre, *Phys. Scr.* **82**, 038111 (2010).

[18] Y. Turek, Y. Li, C.P. Sun, *Phys. Rev. A* **88**, 053827 (2013).

[19] F. Brennecke, T. Donner, S. Ritter, T. Bourdel, M. Kohl, T. Esslinger, *Nature* **450**, 268 (2007).

[20] F. Brennecke, S. Ritter, T. Donner, T. Esslinger, *Science* **322**, 235 (2008).

[21] A.B. Bhattacherjee, *J. Phys. B At. Mol. Opt. Phys.* **43**, 205301 (2010).

[22] W. Chen, D.S. Goldbaum, M. Bhattacharya, P. Meystre, *Phys. Rev. A* **81**, 053833 (2010).

[23] A. Dalafi, M.H. Naderi, M. Soltanolkotabi, S. Barzanjeh, *Phys. Rev. A* **87**, 013417 (2013).

[24] L. Dong, L. Zhou, B. Wu, B. Ramachandhran, H. Pu, *Phys. Rev. A* **89** 011602(R) (2014).

[25] S. Weis, R. Rivière, S. Deléglise, E. Gavartin, O. Arcizet, A. Schliesser, T.J.O. Kippenberg, *Science* **330**, 1520 (2010).

[26] M. Mücke, E. Figueroa, J. Bochmann, C. Hahn, K. Murr, S. Ritter, C.J. Villas-Boas, G. Rempe, *Nature* **465**, 755 (2010).

[27] D.G. Lai, X. Wang, W. Qin, B.P. Hou, F. Nori, J.Q. Liao, *Phys. Rev. A* **102**, 023707 (2020).

[28] A. Muhammad, S. Farhan, *Optik* **125**, 5455 (2014).

[29] T. Wang, M.H. Zheng, C.H. Bai, D.Y. Wang, A.D. Zhu, H.F. Wang, S. Zhang, *Ann. Phys.* **530**, 1800228 (2018).

[30] H.J. Kimble, *Nature* **453**, 1023 (2008).

[31] Y. He, *Phys. Rev. A* **94**, 063804 (2016).

[32] K.A. Yasir, W.M. Liu, *Sci. Rep.* **6**, 22651 (2016).

[33] M. Javed Akram, F. Ghafoor, M. Miskeen Khan, F. Saif, *Phys. Rev. A* **95**, 023810 (2017).

[34] L.W. Liu, D.J. Gengzang, X.J. An, P.Y. Wang, *Chin. Phys. B* **27**, 034205 (2018).

[35] M. Asjad, F. Saif, *Phys. Rev. A* **84**, 033606 (2011).

[36] G. D. Chiara, M. Paternostro, G.M. Palma, *Phys. Rev. A* **83**, 052324 (2011).

[37] B. Rogers, M. Paternostro, G.M. Palma, G.D. Chiara, *Phys. Rev. A* **86**, 042323 (2012).

[38] A. Dalafi, M.H. Naderi, *Phys. Rev. A* **96**, 033631 (2017).

[39] H. Xiong, L.G. Si, A.S. Zheng, X. Yang, Y. Wu, *Phys. Rev. A* **86**, 013815 (2012).

[40] C. Cao, S.C. Mi, Y.P. Gao, L.Y. He, D.Q. Yang, T.J. Wang, R. Zhang, C. Wang, *Sci. Rep.* **6**, 22920 (2016).

[41] C. Kong, H. Xiong, Y. Wu, *Phys. Rev. A* **95**, 033820 (2017).

[42] H. Hao, M.C. Kuzyk, J.J. Ren, F. Zhang, X.K. Duan, L. Zhou, T.C. Zhang, Q.H. Gong, H.L. Wang, Y. Gu, *Phys. Rev. A* **100**, 023820 (2019).

[43] J.H. Li, C.L. Ding, Y. Wu, *Phys. Rev. A* **104**, 063506 (2021).

[44] M. Wang, C. Kong, Z.Y. Sun, D. Zhang, Y.Y. Wu, L.L. Zheng, *Phys. Rev. A* **104**, 033708 (2021).

[45] K. Zhang, W. Chen, M. Bhattacharya, P. Meystre, *Phys. Rev. A* **81**, 013802 (2010).

[46] L.W. Liu, G.H. Zhang, X.J. An, L. Hai, H.Y. Jiao, P.Y. Wang, *Laser Phys.* **29** 065501 (2019).

[47] D. Nagy, G. Szirmai, P. Domokos, *Eur. Phys. J. D* **67**, 124 (2013).

[48] O. Morsch, M. Oberthaler, *Rev. Mod. Phys.* **78**, 179 (2006).

[49] Q. Lin, J. Rosenberg, D. Chang, R. Camacho, M. Eichenfield, K.J. Vahala, O. Painter, *Nat. Photon.* **4**, 236 (2010).

[50] I. Bloch, *Science* **319**, 1202 (2008).

[51] C. Franois, Z. Gergely, S. Pascal, *Phys. Rev. Lett.* **105**, 115301 (2010).

[52] A. Trenkwalder, C. Kohstall, M. Zaccanti, D. Naik, A. I. Sidorov, F. Schreck, R. Grimm, *Phys. Rev. Lett.* **106**, 115304 (2011).

[53] S.B. Papp, J.M. Pino, C.E. Wieman, *Phys. Rev. Lett.* **101**, 040402 (2008).

[54] M. Taglieber, A.C. Voigt, T. Aoki, T.W. Hänsch, K. Dieckmann, *Phys. Rev. Lett.* **100**, 010401 (2008).

[55] H. Jing, X. Zhao, L.F. Buchmann, *Phys. Rev. A* **86**, 065801 (2012).

[56] H. Jing, D.S. Goldbaum, *Commun. Theor. Phys.* **58**, 551 (2012).

[57] L.W. Liu, G.H. Zhang, X.L. Wang, *Laser. Phys. Lett.* **14**, 105201 (2017).

[58] S. Huang, *J. Phys. B At. Mol. Opt. Phys.* **47**, 055504 (2014).